Design of Wings for Jump Gliding in a Biped Robot

by

Vipul P. Gadekar

A Thesis Presented in Partial Fulfilment
of the Requirements for the Degree
Master of Science

Approved July 2020 by the
Graduate Supervisory Committee:

Daniel Aukes, Co-Chair
Timothy Takahashi, Co-Chair
Hamid Marvi

ARIZONA STATE UNIEVRSITY

August 2020

ABSTRACT

This thesis aims to design of wings for a laminate biped robot for providing locomotion stabilization during jump gliding. The wings are designed to collapse down during the jumping phase to maximize jump height and deployed back for gliding phase using anisotropic buckling in tape spring hinges. The project aims to develop a reliable dynamics model which can be utilized for design and evaluation of optimized systems for jump-gliding. The aerodynamic simulations are run on a vortex-lattice code which provides numeric simulations of the defined geometric bodies. The aerodynamic simulations assist in improving the design parameters such as planform, camber and twist to achieve the best possible Coefficient of Lift for maximizing glide distance. The aerodynamic simulation output is then plugged into a dynamics model built in Python, which is validated and correlated with experimental testing of a key wing designs. The experimental results are then utilized to improve the dynamics model and obtain better designs for improved performance. The simulation model informs the aerodynamic design of wings for sustaining glide for the biped platform and maximizing glide length to increase range.

ACKNOWLEDGEMENTS

I would like to express my heartfelt gratitude to Dr. Daniel Aukes and Dr. Timothy Takahashi, my advisors and well-wishers, who gave me a wonderful opportunity to work on this project and guided me through various obstacles. I would also like to thank Dr. Hamid Marvi for his invaluable inputs and assessment of my work.

I would like to thank all my friends and colleagues in IDEALAB at The Polytechnic School, ASU for helping me professionally as well as personally and making the work place a memorable and happy one.

I would not have been here without the incredible love and support from my parents and my family. Thank you for all your motivation and encouragement to pursue my passion for engineering and design. Lastly, thank you to all my friends who have stood beside me through good and bad times.

TABLE OF CONTENTS

Page

LIST OF TABLES

Table Page

LIST OF FIGURES

Figure Page

Figure Page

Figure Page

Figure Page

CHAPTER 1

INTRODUCTION

1.1 MOTIVATION

Recent advancements in robot locomotion have identified jump-gliding to be a very effective locomotion strategy to overcome large obstacles with an optimized application of energy. A body in ballistic jumping motion follows a parabolic trajectory with limited horizontal distance coverage based on its initial velocity, launch angle and body mass with high impact forces on landing. On the other hand, hybrid jump-gliding locomotion can improve the horizontal distance coverage by utilizing aerodynamic surfaces for gliding as well as reduce landing impact forces.

In nature we may observe various aerial hybrid locomotion strategies, traced back to the evolution of vertebrate flight and see how various species adapted to the application of wings in one form or another [1]. It has been hypothesized in some evolutionary theories that the glide locomotion was a precursor to powered, flapping-wing flight due to its inherent simplicity [2]. These have enabled animals to have a better control authority over their body in motion, enhance performance and endurance in running, hopping and jumping as well as dampen the impact forces. We observe that animals in variety of environments such as flying squirrels and flying fish utilize some parts of their bodies as aerodynamic surfaces for improving jump distance and range (Figure 1). Such animals are known to follow jump-gliding strategy to overcome difficult terrain or outrun predators.

Thus, there has been a keen interest in mimicking these biological designs and gait strategies for new robotic platforms to make them more maneuverable and robust.

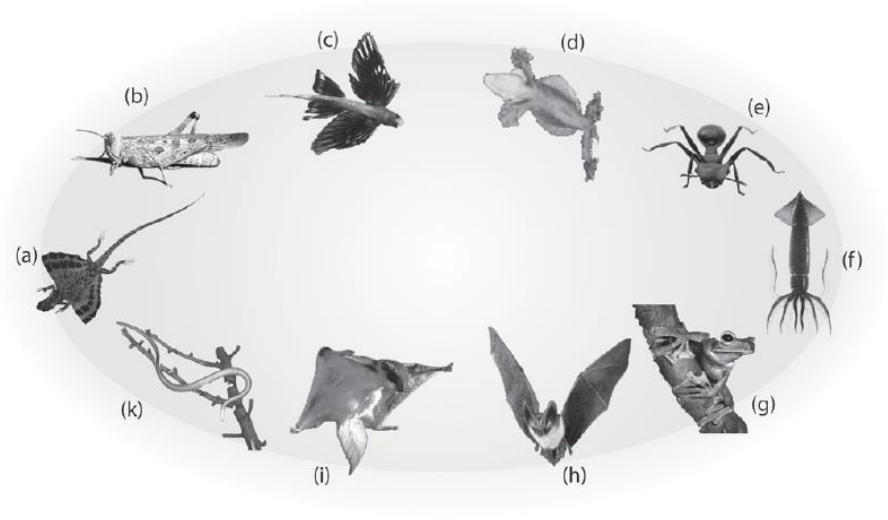

Figure 1: List of biological species utilizing gliding for hybrid locomotion. (a) gliding lizard. (b) locusts. (c) flying fish. (d) gliding geckoes. (e) gliding ants & spiders. (f) gliding squid. (g) gliding frogs. (h) bats. (i) gliding mammals. (k) gliding snakes. [3]

Through numerous studies in robotic design for achieving jump-gliding, a magnitude of mechanisms have been proposed and tested for deployment and stabilization of aerodynamic surfaces. The subsequent sections detail a unique passive mechanism design for deployment of wings and the associated aerodynamic design for achieving jump-gliding. This design work is focused on enabling successful jump-gliding in a biped robot, although the wing design described in this publication can be replicated for any jumping enabled robotic platform. Section 1.2 lays out the problem statement detailing the design principles, platform goals and constraints which govern the major considerations. Section 1.3 introduces current body of work published with respect to the design and

modeling of robotic platforms for jump-gliding. The section also highlights what the author believe are limitations associated with the current work and how they are accounted for in the design proposed in this publication.

Chapter 2 delves into the details of mechanical and aerodynamic design process and the rationale behind the identification, selection and application of tape springs used for deployment of wings. Tape-spring hinges are selected for passive actuation of wings under dynamic conditions due to their characteristic behavior of anisotropic buckling. The application of aerofoil camber and wing planform is detailed in the design of the wing along with the stability considerations. Section 3 details the numeric simulation tools and methodology used for both physics model and aerodynamic analysis. The physics of robot jump-gliding is encoded into a Python based model while the aerodynamic simulations of the wing geometries are analyzed using a vortex-lattice potential-flow analysis code called 'Vorlax'. A complete design workflow is then described which integrates the aerodynamic analysis data into the Python model for design -specific performance analysis. These simulation models are iteratively improved using design enhancement and experimental testing.

Chapter 4 discusses the experimental testing and validation procedure used for correlating the Python model with real-world performance and improving the fidelity of the model. An external launch system was utilized to focus solely on the jump-gliding performance of the wings and reduce any variability in testing. The resulting data is briefed and analyzed in detail with respect to the analytical physics model and glide stability. Lastly, Chapter 5 draws conclusions for the presented data and details a discussion on the

results of the exercise. A brief summary of insights is presented to highlight the various challenges and proposed solutions in the design of wings for jump-gliding, while identifying area of focus for future advancements.

1.2 PROBLEM STATEMENT

Two major areas of research were identified for this thesis: passive deployment mechanism for wings and optimization of the aerodynamic design of the wings for maximum glide ratio. The deployment mechanism is expected to work with minimal components while satisfying the functional and structural requirements of the package[4]. The wing design is aimed to contribute minimal mass to the structure while providing sufficient geometric coefficients to meet the aerodynamic requirements of the robot.

The proposed design utilizes anisotropic tape-spring linkages for collapse and deployment of wings which is detailed in the following chapters. The design of biped wings involved optimizing wing geometry, camber, twist and taper to maximize coefficient of lift. A major physical constraint identified for the geometric sizing of the wings was wingspan. As the wings collapse during the initial jump phase, the length of wing half-span was limited to the height of the biped robot. The mass of wings with respect to the robot mass is also a dynamic consideration for performance and stability analysis. The mass of the robotic platform is assumed to be acting at the center of gravity of the test wings, which is utilized for tweaking the static and dynamic stability in glide phase.

Figure 2: Biped leg design for the robot platform [5].

The proposed design is to be integrated with a two-legged laminate biped robot to maximize locomotion strategies and enhance gait stability (Figure 2). The end goal of the project is to design a package that can be tuned structurally and aerodynamically to maximize jump-gliding for any given robot.

1.3 LITERATURE REVIEW

A large number of robots that incorporate biologically inspired jump-gliding strategies have been investigated for improving efficiency and range of robots. A number of studies published in recent years have primarily focused on miniature multi-legged jumping robots with distinct wing-deployment mechanisms. Robots designed with deployable wings utilize various active-actuation mechanisms such as servo motors, worm gears or string muscles across the range of robot sizes. Kovac, et al. [3], detail the exploration of various robotic systems for jumping and wing-deployment for gliding. The

authors conduct a review of different types of system designs resulting in the design of EPFL 16.5 gm. jump-glider presented in [6][7]. The authors have detailed the comparison of design, analysis and functional operation of small jump-gliders with fixed and foldable wings. The authors conclude that the additional weight of any mechanism aimed at deployment of wings after the jump phase can negatively affect the performance of the robot and thus favoring fixed wing configuration, especially for jump-gliding from an elevated position. This paper includes evaluation of three distinct wing deployment mechanisms including a butterfly-inspired design, which is very similar to the wing deployment strategy presented in this thesis. They argue that butterfly inspired designs such as this reduce jump height due to their reliance on aerodynamic friction. While that evaluation might be true for the miniature EPFL jump-glider, the same reasoning necessarily does not hold true for larger robot platforms. Moreover, the design presented in this thesis utilizes aerodynamic drag force to collapse wings via the anisotropic buckling of tape-spring hinges, lowering drag force requirements.

In a locust-inspired jump-glider presented by Beck, et al. [8], the deployment of wings is actuated using a small worm gear mechanism. The wings sweep back to be parallel to the body during jumping and then deploy after the leap. This miniature robot weighs only 25 gm and uses an accelerometer to identify the end of the jumping phase; the wing deployment is time triggered using experimentally derived values. This paper is based on a jumping robot presented in [9] and focuses on the utilization of aerodynamic surfaces for in-flight roll, pitch stabilization and yaw control. The robot has folding wings with a small 30 cm wingspan and a small horizontal stabilizer tail.

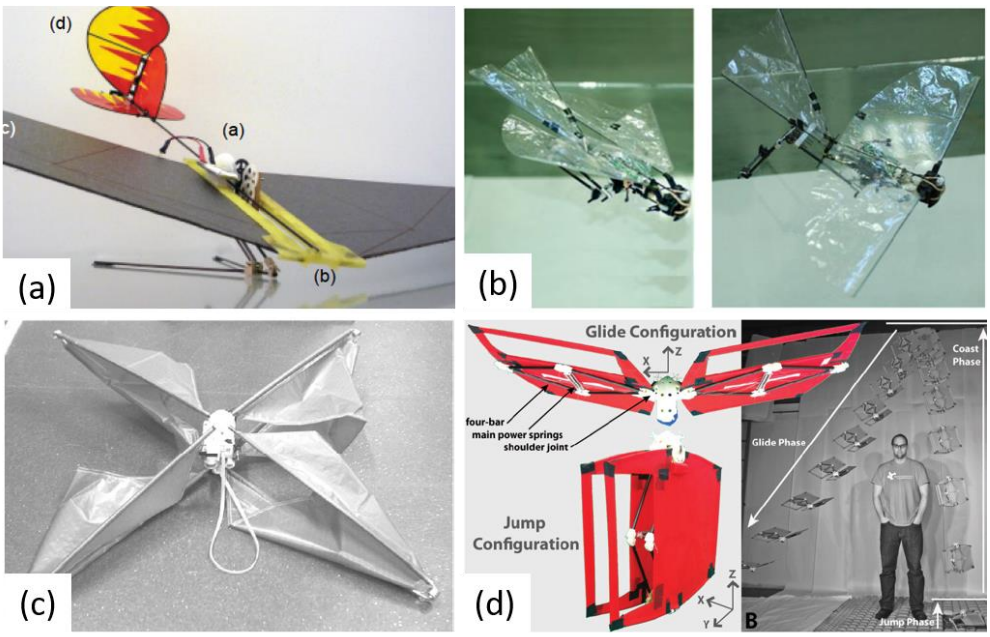

Figure 3: (a) EPFL fixed-wing jump glider [4]. (b) TAUB locust inspired jump glider[8]*. (c) Glumper*[10]*. (d) Multi-Mo bat inspired jump glider*[11]*.*

In [12], Desbiens et al. detail the design of a 67.5 gm jump-glider robot capable of autonomous repeated jumps with a pivoted wing for deployment. The paper delves into the detailed analytical model including Cost of Transport formulation, developed for simulation of multi-physics jump-gliding dynamics and how the resulting equations inform the design of the robot. The wing and horizontal stabilizer are designed to align with the air flow direction during the jump to minimize the aerodynamic drag. At the apex of the leap, the wing is locked in the horizontal position using an actuator to be effective for the glide phase. The robot is especially focused on maximization of gliding distance, as evident from the large dimensions of the wings with respect to the robot with 1.12 m wingspan and 15cm wing chord. While the wing deployment mechanism is aimed at reducing aerodynamic drag by adjusting the relative angle of attack of the wing with

respect to air flow during different phases of jump-gliding, the construction of pivot restricts the robot's launch angles. They conclude that for effective jumping in any robot, it is important for the launch angle to provide enough ground friction such that no energy is lost in slippage at the ground contact points requiring steeper jumps from robot. Moreover, the wings designed in this robot use flat-plate geometry which require larger wingspan and aspect ratio to generate enough lift force.

Armour et al. have presented a different type of jump-gliding robot named 'Glumper' in [10]. The robot weighs 700 gm and uses four legs with torsional springs located at the hinge for jumping and sail-like membranes attached to the legs for gliding. The membranes act similar to parachute sections which are automatically deployed with extension of legs during launch. The robot is designed to re-orient in flight by shifting its mass to affect the angle of attack. Although the robot does not utilize any active actuation for wing deployment, the need for active flight stabilization makes this system complicated. Moreover, the experimental results presented in the paper show that the robot's range is lower with wings than otherwise.

Woodward and Sitti [13] presents a detailed design for a bat-inspired wing morphing robot weighing 115.6 gm. The four-bar leg linkage mechanism for jumping gaits is shared with the wing structure. After the jump phase, the wings are deployed using compression cables which actuate the leg linkages at the shoulder joints for gliding phase, which is a clever implementation of biological skeleton structure of a bat. The paper highlights experimental testing with placement of Center of Mass (COM) with respect to wing chord for passive flight stabilization and rate of spring stiffness at shoulder joints for

wing deployment. The wing membrane is made from ripstop nylon material and use of curved beam shape and provides a healthy airfoil shape to the wings. It can be observed that every jump gliding robot has utilized a different actuation strategy and thus opportunities exist for innovative mechanism design and system integration for successful robot performance.

While in theory, actively actuated mechanisms provide greater closed-loop control over the deployment of wings, previously reviewed research studies highlight the mass penalty of active actuation mechanisms. The robot platforms presented above are primarily designed and analyzed for the jumping strategy. Fewer robots capable of multi-gait strategies such as walking and jumping in conjunction with wings have been developed. Some exceptions include such as [11], which presents a bat inspired robot which applies adaptive morphology to showcase multi-modal locomotion. The wings are designed to morph for legged locomotion such as walking while a dedicated motor propulsion is present for flying. There has also been an interest in augmenting the multi-legged robots with ornithopter inspired flapping wing mechanism along with jumping, walking gaits as presented in [14] [15].

In this study, design of a wing system for hybrid locomotion of jump-gliding in a laminate biped robot presented in [5],[16]. The biped robot platform is designed to operate with multiple gait strategies such as walking, running, hopping and jumping, using its 3DOF kinematics in conjunction with tuned dynamics. Our aim is to further enhance the gait capabilities of this biped platform by utilizing wings with s compliant deployment mechanism. This will not only enable the robot to extract jump-gliding capabilities but

will also assist in gait stabilization and performance enhancement during running and hopping. Halden, et al. use the application of aerodynamic surfaces in multi-legged robots for dynamic locomotion stability as presented in [17]. Their work presents an additional advantage of having rigid aerodynamic surfaces for rotational stability against perturbations and to increase robustness for terrestrial locomotion. This study only focuses on the design of wings for jump-gliding locomotion while the effect of wings on rest of the terrestrial gaits is left for future consideration.

The majority of published work on jump-gliding have primarily assumed flat-plate wing geometries for simplification of design and model analysis. While the flat-plate geometries simplify aerodynamic analysis of the robot model, there is scope for increasing the performance of these wings by application of wing camber, twist to maximize the glide range. The author has not been able to trace any study focusing solely on the aerodynamic design and integration of the wings for jump-gliding robots. Thus, this paper aims to present a detailed aerodynamic design of wings and their effective dynamic deployment mechanism using passive actuation for jump-gliding. This publication expands on the preliminary study and experiments presented in [18] by Guston Lighthouse and Daniel Aukes, which have successfully shown the application of tape-spring hinges in jump-gliding for dynamic wing actuation.

CHAPTER 2

DESIGN

2.1 Tape Springs

Tape Springs are thin-walled, straight shell beams with lateral curvature. They are commonly found in tape measures, also called as Carpenter's tape, wherein they are coiled around inside a plastic case. The lateral curvature of tape springs results in peculiar elastic dynamic behavior which can be utilized in different applications for passive deployment actuation. A zero-load, zero-strain tape spring can be defined by the width of the tape, the wall thickness of tape, the radius of lateral curvature and the angle subtended by the arc thus formed. The tape springs have an elastic tendency to return to zero-strain, straight level state when deformed, either by local folds or by coiling. Although coiled tape-springs have been studied in depth especially for application in spacecraft deployment[19], we will concentrate only on the bending behavior of tape springs loading. The elastic behavior under load bending in tape springs is non-linear and different for the two directions of displacement. The tape spring can be displaced be in equal-sense bending when bent towards the concave curvature of the shell and in opposite-sense when bent in the convex direction of the curvature. The folding behavior highlighted by the moment-rotation diagram in Figure 4(c) illustrates the two-dimensional, asymmetric elastic folding in a single tape-spring element. The tape-spring element has a much bigger maximum moment in opposite-sense bending than that in equal-sense bending, which is utilized for wing deployment, as presented in this publication.

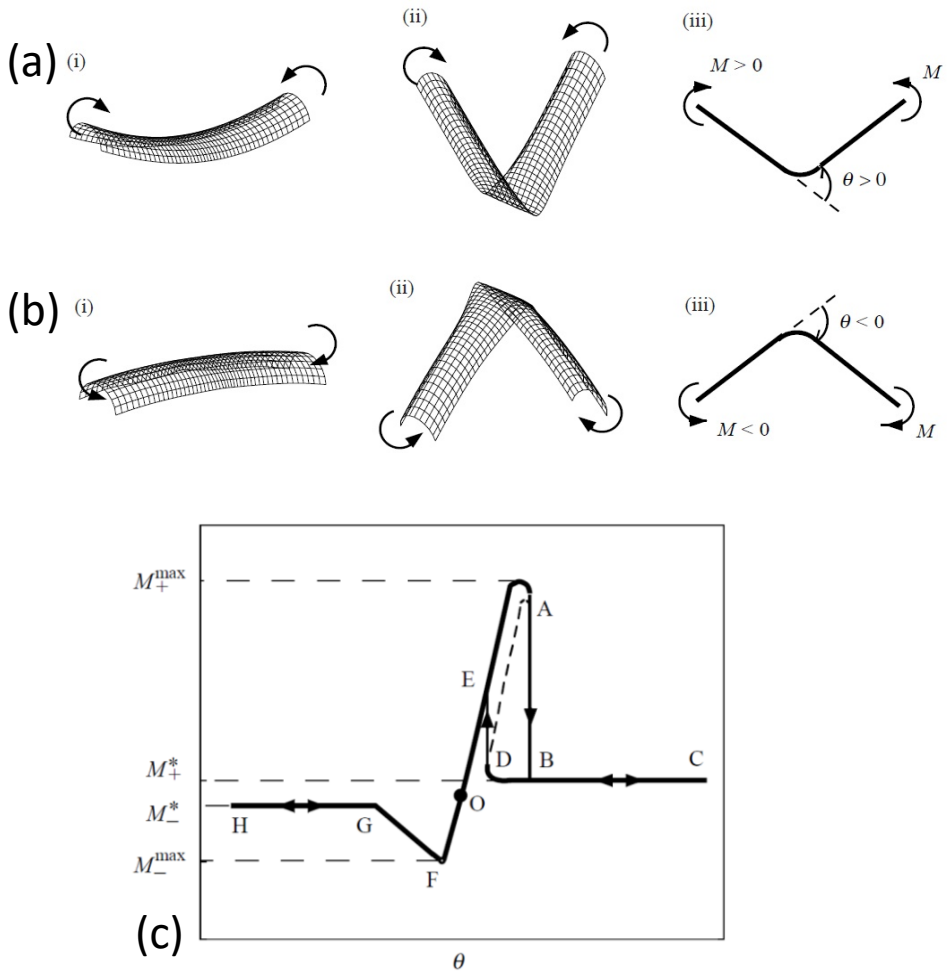

Figure 4: (a) Opposite Sense bending in Tape Spring. (b) Equal Sense bending in Tape Spring. (c) Theoretical Moment- rotation relationship [20]

The wing deployment proposed in this publication exploits the difference between the maximum supported moment in opposite-sense and equal-sense bending to control the direction of folding of the element. For a given tape-spring element in equal-sense configuration, any applied moment greater than M^* will result in beam buckling in equal-sense direction. If the same applied moment at any given time is sufficiently less than the opposite-sense maximum moment, we can control the rotation behavior of the tape-spring

in one direction. The same principle is used in the presented jump-glider for collapse of wings during the jump phase and self-deployment of wings for the glide phase.

The wings are connected to the robot platform using multiple tape-spring elements. All the elements are arranged so as to be in the equal sense bending configuration. When the robot begins to jump, the relative air velocity acting on the wings generates aerodynamic drag force, pushing down on the wing surface. This negative moment is utilized for folding of the tape-spring elements in equal-sense, thus collapsing the wings and decreasing the air resistance due to the reduced apparent wing surface area. The strain applied by this drag force is stored in the tape-spring elements. This is important for the robot to achieve a jump height higher than what could be achieved with non-collapsible, fixed wings. When the robot reaches the apex of the jump, the robot loses all its kinetic energy and vertical velocity components become zero. As the applied moment loads on the wing vanishes, the stored strain energy is released and the tape-springs self-deploy, returning to their neutral configuration. Due to the self-deployment behavior of the elements, the transition phase from jumping to gliding phase can be very quick. The robot transitions into the gliding phase as soon as the wings are deployed at the jump height, without any external actuation. During the gliding phase, the lift force generated by the wings exerts a positive moment on the tape-springs. The folding of tape-spring elements in the opposite-sense is avoided by careful study and analysis of the generated lift force, which is discussed next, in section (2.2).

The tape-spring used for the study and experiment in this project were hardened-steel elements taken directly from a tape-measure. The moment-rotation relationship was

experimentally determined using a 90mm long element shown in fig.5. The experimental result provided a design range of moment loading for the actuation of the tape springs, which was used for modeling and tuning of the wing deployment system. The equivalent torsional spring stiffness of the tape-spring 2D elastic fold was calculated using Hooke's law:

$M = (k^* \theta)$

where k = torsional spring stiffness;

θ = rotation angle, calculated in anti-clockwise direction from horizontal axis

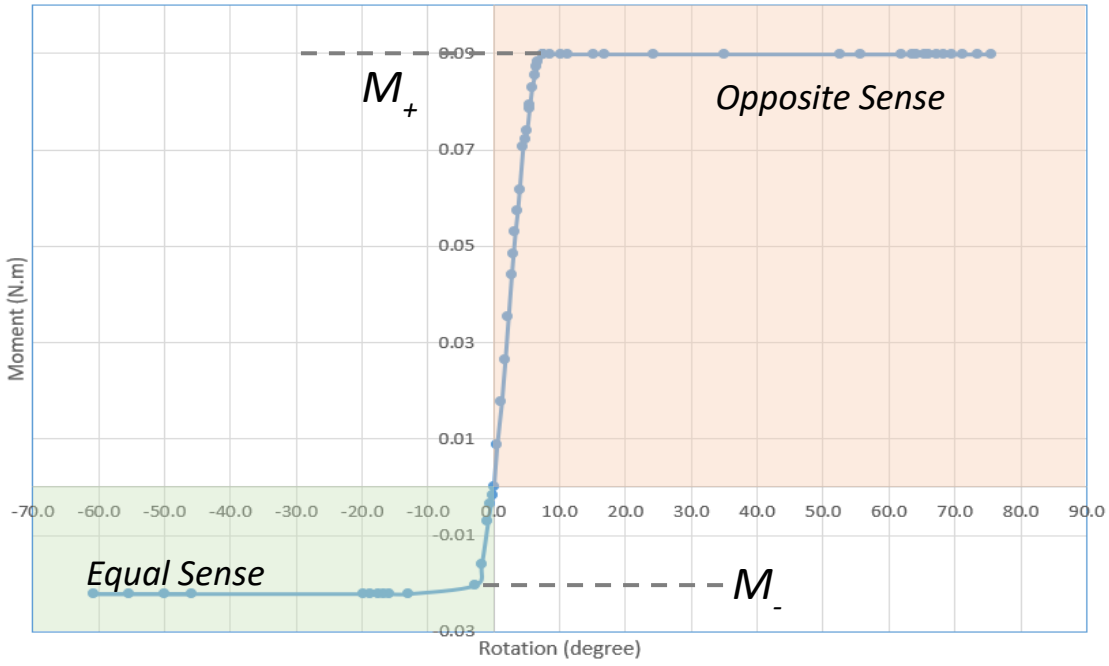

Figure 5: Moment- rotation relationship of the applied tape spring linkage determined experimentally.

For simplification of model, only three distinct points in the moment-rotation curve i.e. spring stiffness at maximum equal-sense moment, spring stiffness after equal-sense

bending and spring stiffness at maximum opposite-sense moment, were used for modeling the behavior of tape-springs in response to the aero forces.

Application of tape-spring elements for actuation and self-deployment provide several major advantages. The whole mechanism is very simple mechanically but can be tuned for specific design domains with much ease. The mechanisms utilize the natural compliance in tape-springs without any extra additional components. The folding and deployment of the tape-spring, especially in equal-sense configuration, is very quick and predictable. Although the proposed wing mechanism does not enable in-flight dynamic control, it is easier to assemble and prototype.

2.2 Aerodynamic Design

A body in motion through any fluid has four fundamental forces acting on it: Thrust, Drag, Lift, Weight. For a body in motion through air, equipped aerodynamic surfaces generate lift and drag forces while the thrust force is applied by some external mechanism, usually propulsion engines. A body is said to be in gliding motion when the thrust force is absent, and the body continues its flight by the lift force opposing the weight. In order to generate lift force, the glider must remain in motion at some velocity, which also generates drag force. The generated drag force is responsible for slowing down the velocity of the body by dragging it backwards and thus a body in gliding motion loses its ability to generate sufficient lift over time, sinking down due to the body weight. The aerodynamic surfaces on the body directly affect the generation of lift and drag forces. For a flat plate moving

through the fluid, the attitude of body with respect to the air velocity causes an effective angle of attack (A.O.A) which leads to different pressure regions being created at the top and bottom surfaces.

The aerodynamic design of our jump-gliding wings followed the geometric and operational constraints posed by the biped platform [5]. The aim of the thesis was to generate sufficient lift for carrying the biped platform through glide phase, while satisfying the moment requirements of the tape-spring hinges for collapse of wings. The velocity regime for the operation of wings was based on simulation information from [5] as well as initial design calculations. It was found that the wings were to operate in the range of 2 m/s to 8 m/s. These values were then used to calculate the Reynolds number (Equation 1) for the wing root chord length of 180 mm as well as the wing tip chord length of 60 mm to gauge the complete spectrum of flow conditions (Table 1).

$$Re = \frac{\rho * v * L}{\mu} \tag{1}$$

Velocity (m/s)	Wing Chord Length (m)	Wing Reynolds number
2	0.18	2.38E+04
5	0.18	5.96E+04
8	0.18	9.54E+04

Table 1: Calculated Reynolds number for generated wing design.

It was important to understand the Reynolds number regime for the wing for application of VORLAX code. VORLAX is a potential-flow code which assumes inviscid, irrotational flow. The potential-flow assumption dictates that the operating Reynolds number must be higher than 1e06 to accommodate the assumption of near zero fluid viscosity. Although it

has been shown that the potential flow analysis can be applied to fluids with Reynolds number higher than 1e04, but with some caveats. From Table 1 we can see that the lowest operational Reynolds number for the wing is 2.38e04, which allows us to use the potential flow analysis tool with some precautions. A mean velocity of 5 m/s was used for analysis of wing geometries in VORLAX.

It was clear from initial design studies that a flat-plate wing would not be able to provide sufficient coefficient of lift (CL) for maintaining successful gliding. Thus special efforts were diverted towards application of camber and wing planform to meet this unusually high CL demand. During an unpowered glide phase, the ratio of vertical height lost to the horizontal distance covered is called as Glide Ratio. The glide ratio represents the efficiency of glider at covering given horizontal distance at the expense of altitude. For a glider to be successful, the glide ratio should be as high as possible for the given mass, which can be achieved by a high Lift/Drag ratio. A high L/D ratio can be achieved by either greatly reducing the drag generated by a body in flight or by increasing the lift force generated by the aerodynamic surfaces. In case of our system, the drag contribution by the bipedal legs of the platform will vastly exceed any induced drag generated by the wings. Hence, the wings are designed for generating maximum possible lift force by attaining maximum CL value for the given geometric area. The drag contribution of the wing is utilized for collapse of tape-spring hinges during jump phase.

It was important to analyze multiple wing designs for resulting CL, CD values at given velocity and angle of attack (A.O.A) regimes before design selection. A numerical

simulation code based on vortex-lattice method called VORLAX was used for aerodynamic analysis of each design, as detailed in Section 3.1.

Wingspan (meters)	Wing Root Chord (meters)	Wing Tip Chord (meters)	Wing Area (meter^2)
0.7	0.18	0.06	0.1008

Table 2: Final dimensions of the generated wing design.

2.2.1 Wing Planform

The shape of the wing when viewed from the top is called as planform. It was noted early on that the robot in jump-gliding phase had more in common with the sport of hang-gliding than any other system, as in both cases the wings are to hold and dynamically balance a considerable amount of mass below the centerline. As discussed in [21], most of the hang glider designs prevalent today follow what is called ‘Rogallo Wings’. Rogallo Wings are flexible wings made by wrapping a textile skin over wing structure, shaped in a triangular delta planform or diamond planform similar to kites. Rogallo Wings are favored in the sport of hang-gliding for their smooth stability and control in a modular, stowable package. While a delta planform wing was analyzed in preliminary study, it was not selected due to the reduced wing area. As mentioned previously, the wings are allowed to have total wingspan based on the total leg height of the biped platform to ensure wings do not interfere during the regular gait cycles. Thus a rectangular area was identified as allowable design space. It was important to utilize as much area as possible so that the required CL could be reduced for generating the required amount of lift.

When the rectangular planform is modified slightly to have a smaller chord length at the wing tips than the root, it is called a tapered planform. The tapered planform provides better aerodynamic air flow characteristics and dynamic stability against a rectangular wing of same surface area. It is much more important to have a suitable taper ratio wing designed for managing the spanwise flow of air over a highly cambered wing like in our design. The details of VORLAX simulation results and analysis over different wing design iterations is presented in Section 3.1.

2.2.1 Wing Camber

A flat-plate is not very efficient at generating lift force, especially with respect to increasing angle-of-attack. While the theoretical maximum coefficient of lift attainable for a flat-plate is known to be around 6.283, it is very difficult to reproduce in real flight[22]. Thus, camber is introduced to aerodynamic sections which help in tuning the wing aerofoil sections to generate efficient lift[23]. Although a detailed database of camber performance for numerous aerofoil sections exist, the camber can be further tuned and designed for specific wing geometries, velocity regimes or angle-of-attack. The introduction of camber further widens the difference in pressure gradient between the top and bottom surfaces, thus creating greater maximum CL values at specific velocity and angle of attack intervals. The camber profile for any given section can be defined by two variables: Maximum camber (in percentage with respect to chord length) and Location of Maximum camber (in percentage with respect to chord length). The aerofoil sections in existing standard databases have a maximum camber of about 9-12% for use in gliders and other low Re

wings. Further increase of camber in such applications results in massive air flow separation due to the extreme curvature of the wings. Thus, the design of wing camber is a powerful tool in generation of required lift force for any aerodynamic application by placing these maximum CL numbers in the desired operating domain of the body.

The preliminary study for jump-glider wing camber investigated several camber profiles for their maximum CL output using VORLAX at a constant air velocity of 5 m/s. The analysis included various airfoil camber sections from standard database as well as a few modified sections for higher camber. The camber profiles considered in the study are highlighted in Figure 6(a). There was a direct relation between the maximum applied camber and the resulting maximum CL value (Figure 6(b)) which prompted in the selection of 20% maximum camber airfoil section.

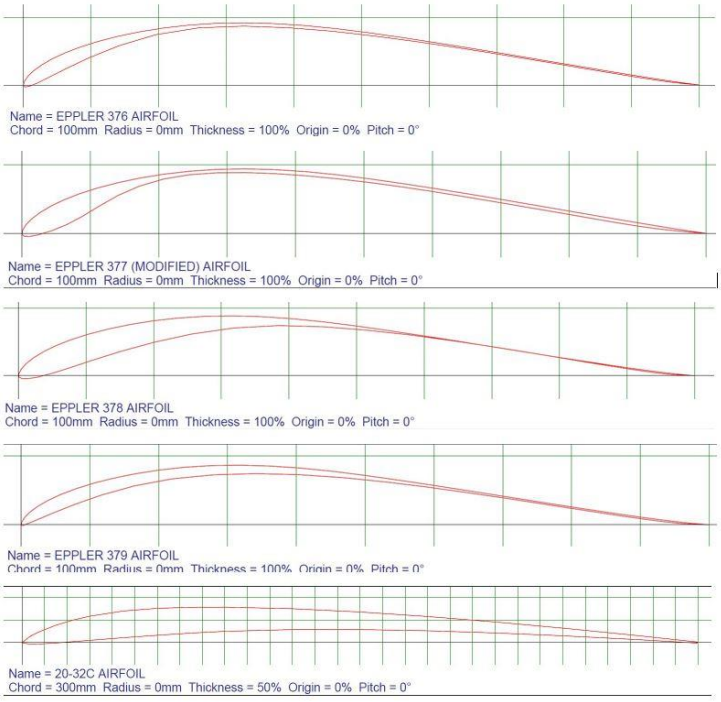

(a)

(b)

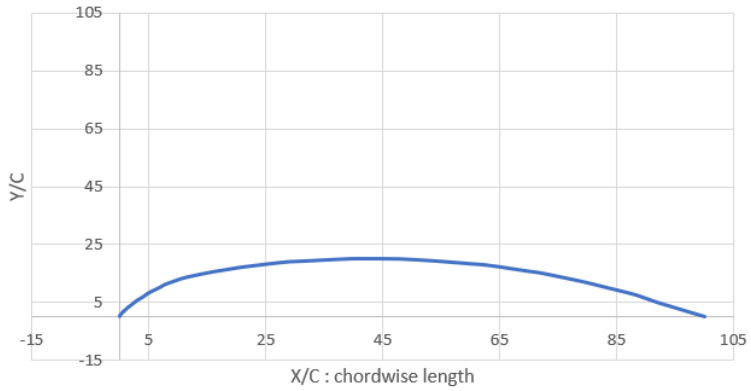

Figure 6: (a) Camber profiles analyzed for initial design studies. (b) Purpose-made airfoil with 20% camber profile.

The application of thickness was avoided in the design and analysis of these section due to practical reasons. The thin, single-surface sections need less construction material which resulted in lighter wings as opposed to thicker airfoil sections. Thus, the aerodynamic analysis was adjusted accordingly in VORLAX input files. The final wing design is detailed in Chapter 3 with regards to VORLAX simulation as well as in Chapter 4 with respect to prototype testing and validation.

2.2.2 Aerodynamic Stability

The flight stability of the wings during glide phase is an important component of the design process. A traditional airplane achieves flight stability by balancing the aerodynamic forces and the resultant moments with respect to the center of gravity for the motions of Roll, Pitch and Yaw. The lift force generated by the main wing is balanced by the moments of opposing aerodynamic force by the aft horizontal stabilizer. Although the aft tail provides easier flight stability and control, there was a major drawback identified

with using such a configuration for the jump glider. The existence of aft tail in jump phase would negatively affect the jump height due to additional air drag force. Moreover, the aerodynamic surface area required for the tail to generate effective balancing moments was too large, further increasing the air resistance. Thus, the positive stability is derived only from the wings, as case in tail-less flying wing aircrafts and hang-gliders [21][24].

The analysis was focused on only pitch stability of the system. It is assumed that there is no motion in roll and yaw axis for modeling purposes. The pitch stability is highlighted due to its direct contribution in gliding performance as well as the jump integration for the bipedal robot. The aerodynamic stability design is based on the location of three variables, namely Center of Gravity (C.G), Center of Pressure (C.P) and Aerodynamic Center (A.C).

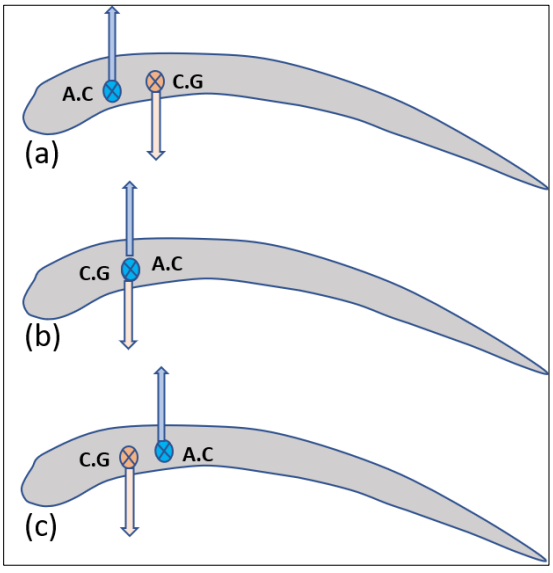

Figure 7: (a) Unstable pitch stability to forwards A.C. (b) Neutral Pitch stability. (c) Positive Pitch stability with aft A.C.

The C.P is the point in space where all the moments resulting from aerodynamic forces is zero. Thus, any aerodynamic force can be modelled to be acting at the C.P for analytical

and simulation purposes. To attain a level flight with no inputs required, also called as Trimmed Flight, it is important that the location of C.P is coincident with the C.G. This allows the longitudinal moments to zero out. The A.C is the point on the longitudinal axis of the wing where the aerodynamic moments remains constant with changes in lift force. A Neutral Point (N.P) is a point on the longitudinal axis of the body where the placement of C.G will result in a neutrally stable body[25]. For our wing-only system, the A.C is same as the N.P. Thus, if the C.G of the body is coincident with the A.C, the body is said to be in static neutral stability. For such a configuration, any external perturbation applied to the body will cause it to react away from its previous path and then maintain this new attitude until another external force is applied. A positive stability is achieved when an external perturbation causes the body to deviate from its pitch attitude momentarily, before coming back to level flight. It is imperative to position the C.G ahead of the A.C such that any perturbations will result in the opposing moments which will restore the system back to its original attitude[25].

In traditional stability analysis, analytical or otherwise, it is assumed that the airfoil is mildly cambered and the C.G lies closer to the longitudinal plane of the plane. Both these assumptions are voided in the design of our wing system due to extremely high camber and the low-hanging C.G caused by the dangling bipedal legs of the robot. Hence, the stability and control of hang-gliders is studied as presented in [24]. The low-hanging C.G induces a special phenomenon. Thus, there is special care taken during the analysis of VORLAX output results for pitch coefficients and resulting locations of C.P, A.C.

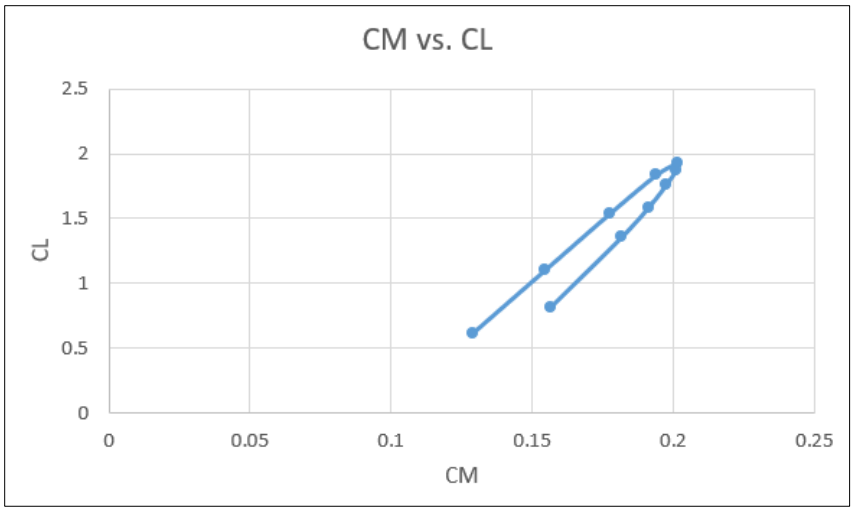

Figure 8: Relationship between Coefficient of Lift and Coefficient of Pitch Moment for understanding static longitudinal stability of the wing geometry.

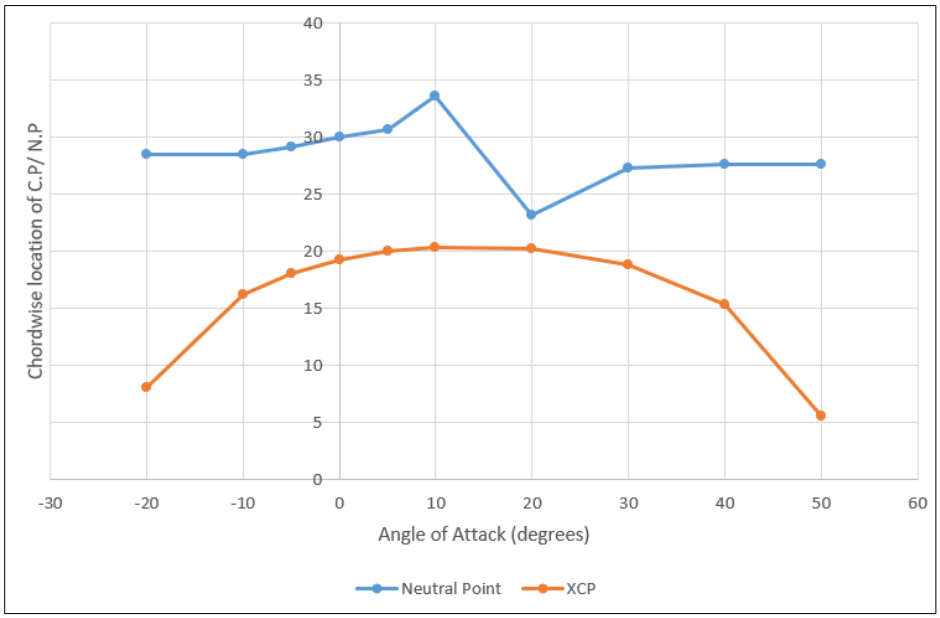

Figure 9: Location of Center of Pressure and Neutral Point for the wing geometry.

CHAPTER 3

SIMULATION

3.1 VORLAX

VORLAX is a potential-flow based numeric tool for aerodynamic analysis of geometries using specially designed vortex lattice panel method. The tool is easy to use due to its basic numeric structure and is known to be accurate within the limitations of basic theories. The code was developed and published by L. Miranda et al. [26]. The code uses simple input structure for geometry design and definition for all wing and fuselage structures along with the analysis configuration such as velocities, angle of attacks etc. The code is then fed into the numeric solver to provide two main sets of results: the force-moment coefficients of lift, drag and pitch along with the local pressure distributions for each grid point. As the code is based on the potential flow theory which assumes the fluid flow to be inviscid, the drag data obtained from VORLAX does not include any skin friction drag component.

Utilizing such a numeric analysis tool provides major advantages of fast processing time and rapid design iterations based on analysis. The tool can also be embedded and codified into the design workflow for creating a single platform for geometry definition and analysis of results. The numeric nature of output also results in comparatively easy implementation of the aerodynamic data into other platforms such as Python in case of this project.

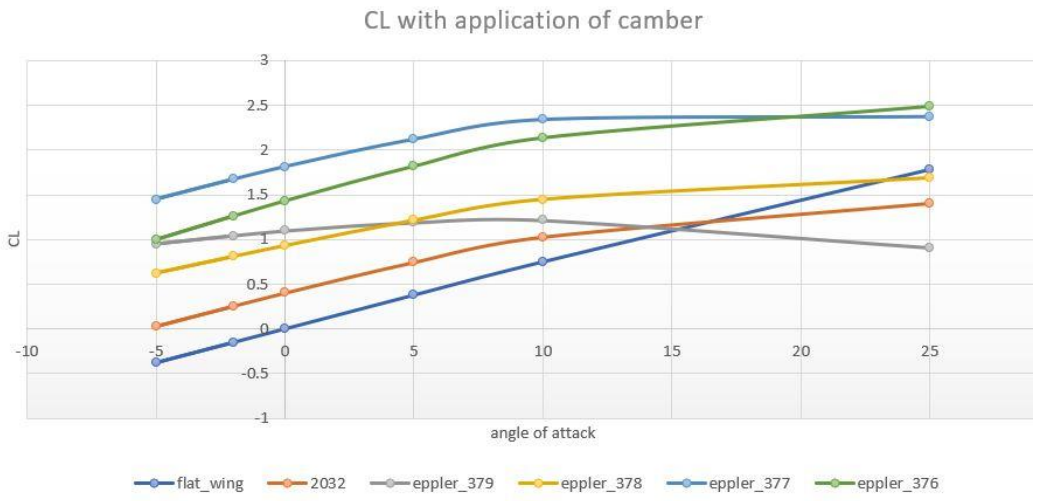

Figure 10: Initial design analysis of standard aerofoil sections.

The wing geometries defined for the project were based primarily on planform and camber, as discussed in the previous chapter. The initial design study included testing the output results for various camber profiles over a rectangular wing to understand the lift performance of the profiles. The standard airfoil database from [27] and [28] was used for identifying high-lift airfoil profiles for the initial study, which were analyzed for their maximum coefficient of lift in VORLAX. The design study camber profiles are illustrated in Figure 6 (a). It is evident from the output in Figure 10, that higher camber a profile has with reduced thickness, it can generate higher maximum CL. The highest camber profile was identified to be Eppler 377 profile with its highest camber of 9.2% of chord, a bulging leading edge and a very thin aft body. The wings are to sustain a biped platform weighing around 1kg. in glide phase at very low speeds of around 3-5 m/s. This meant for the wing to produce 1kg. of lift at 5m/s. the required CL was around 3. Thus, even the best performing camber profile from the study was not able to meet the CL requirements. It was thus decided to modify the camber profile and increase the maximum camber upto

20% chord. This was done by carefully incrementing the (X, Y) coordinate data from a basic Eppler 377 profile and massaging the curvature of the profile to produce a newer airfoil section presented in Figure 6 (b). The new camber profile was also reduced to a single panel, meaning an analytical zero thickness airfoil for practical purposes. The resulting airfoil produced a peak CL of around 3.5 with the similar wing geometric dimensions. It was important to have a high-lift, high- camber airfoil to operate in the very low-speed regime with a heavy robot payload.

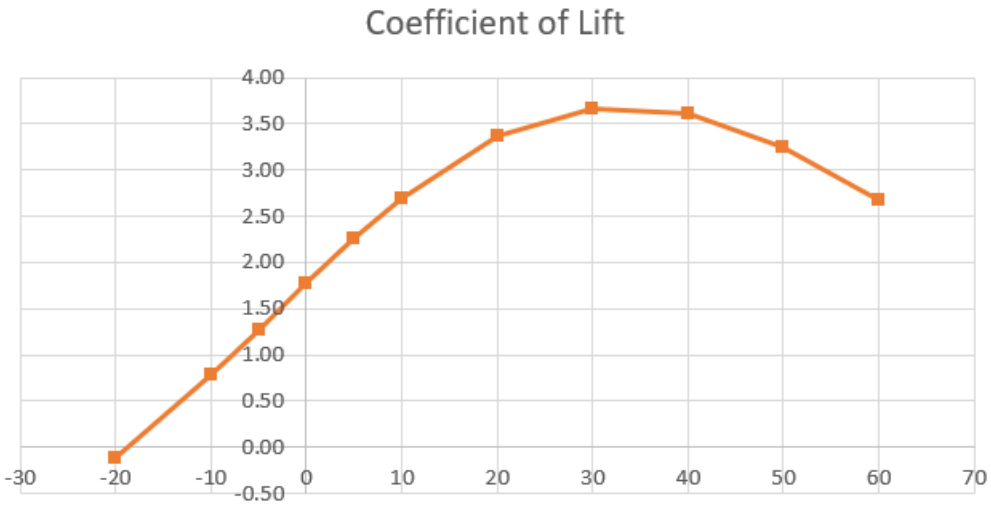

Figure 11: Aerodynamic analysis for the generated camber profile.

After selecting the camber profile, design analysis was done on the planform configuration of two wing shapes: Rectangular Wing and Delta Wing (Figure 12). The rectangular wing was designed with a smaller wing tip chord to manage spanwise lift distribution. The delta wing has an inherent sweep angle associated with it and it was decided to test the wings with leading and trailing edge sweeping to maximize the surface area within the wingspan length constraint. The analysis study also included the

application of wing tip twist, which helps in avoiding the wing tip stall and making the wing more aerodynamically compliant. The design study also included the analysis of location of C.G on the pitching coefficient (CPM) of the wing by defining the X reference point and Z reference point for the wing design in VORLAX. All the wing designs had constant 20% camber profile applied to them, with a delta wing teste for flat-plate profile and each configuration is detailed in Figure 11.

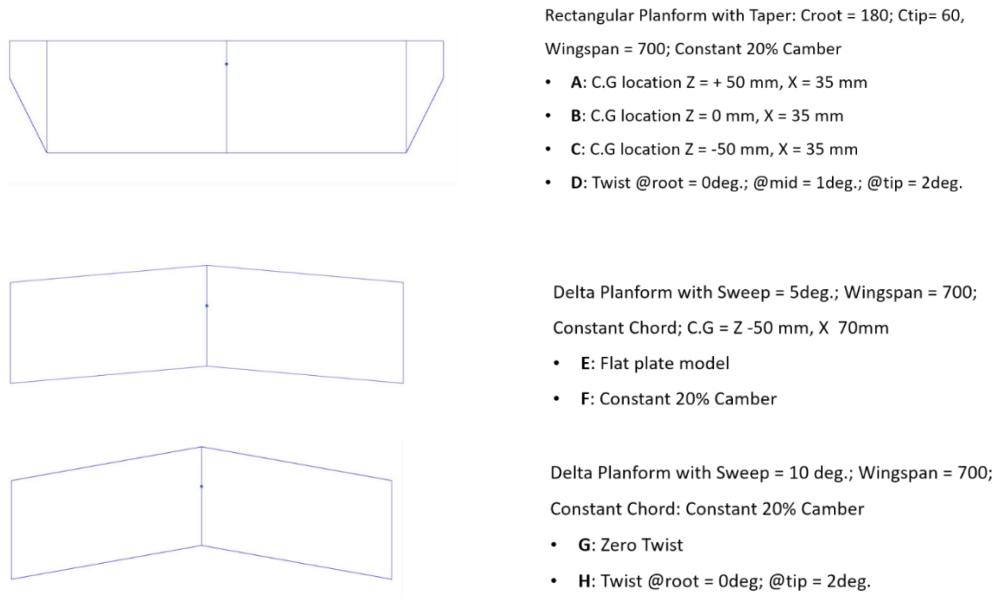

Figure 12: Wing design iterations generated for aerodynamic analysis.

As is evident from the results (Figure 13, 14, 15), the rectangular planform iterations outperformed all other configurations for max. CL output. It can be observed that the wing twist does reduce the max. CL output when compared to other rectangular planforms, but it is better for reducing CD and has better CPM across alpha. The delta wing planform configurations perform better than rectangular wings for CD, but are less favorable for max. CL, which is the design focus for this project. Hence, the tapered

rectangular wing planform with 20% camber profile is chosen for further design, analysis and testing. The wing twist is not applied to the subsequent designs due to the complexity in producing an accurate twist profile in test articles for experimentation.

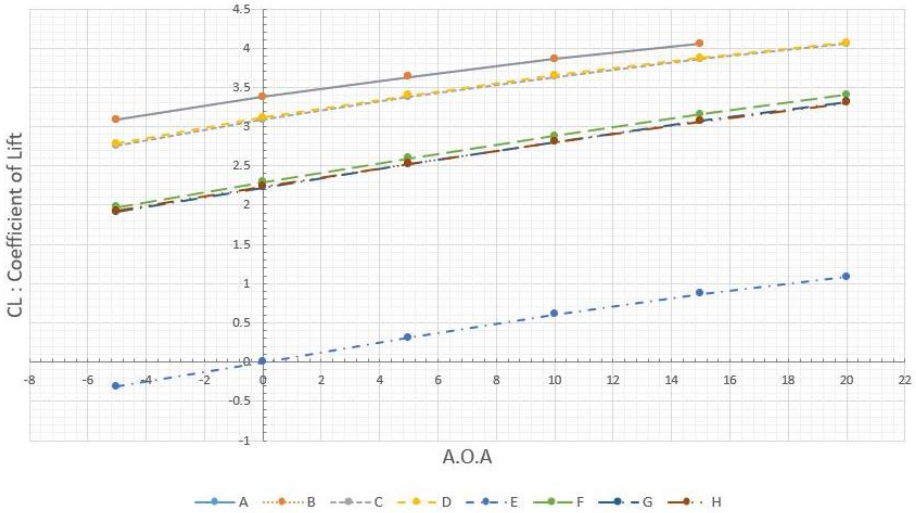

Figure 13: Coefficient of Lift for the analyzed design iterations.

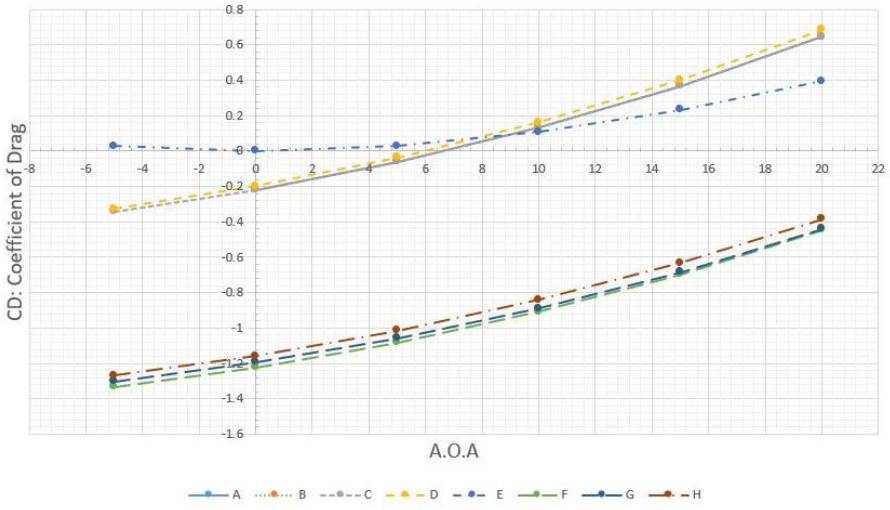

Figure 14: Coefficient of Drag analysis results of wing design iterations.

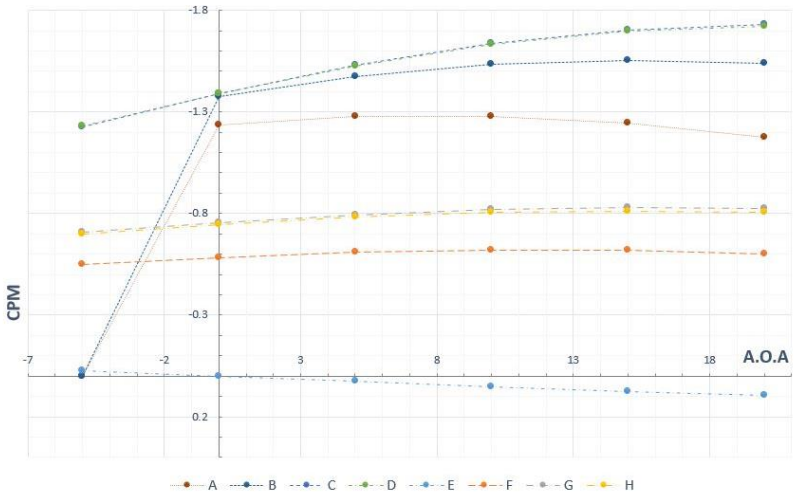

Figure 15: Coefficient of Pitching Moment analysis results of wing design iterations.

The pressure distribution data from the VORLAX output was plotted for each angle of attack, presented in Figure 16. It is important to remember that the VORLAX is a attached flow simulation tool, meaning the VORLAX output results for CL/CD will assume there is no separation in air flow over the wings at all speeds and all angles of attack. This is however not the case in reality, especially with such high cambered profile. Moreover, the previous caveats of potential flow assumptions at these low Reynolds number need to be considered. Thus, to identify the air flow separation over the wings, Thwaites equation was used which presents a formulation for lambda, the laminar separation criteria using the thickness of laminar boundary layer (d_2) and the indicated surface velocity (V).

$$d_2 = \frac{0.664x}{\sqrt{Re}} \tag{2}$$

$$V = Ma\sqrt{1 - CP} \tag{3}$$

$$\Lambda = \frac{\rho d_2^2}{\mu}\frac{dV}{dx} \tag{4}$$

The criteria indicate that if the numerical value of lambda (Λ) is less than -0.09, stall will occur[29]. This criterion was used to plot the separation of fluid presented in Figure 17. It can be seen that the maximum air separation occurs at the trailing edge on the airfoil at negative and low positive angles of attack. The air flow starts to separate near the middle wing just fore of the trailing edge at higher angles of attack due to the high camber.

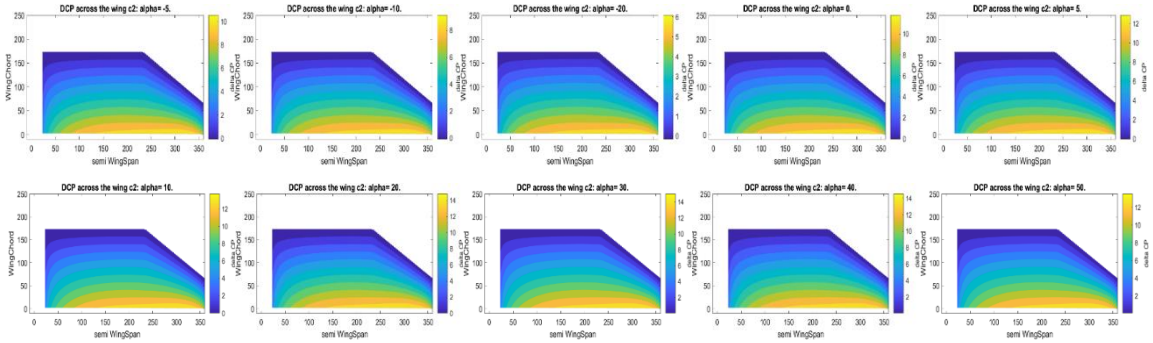

Figure 16: Distribution of pressure coefficients over the wing across the angle of attack.

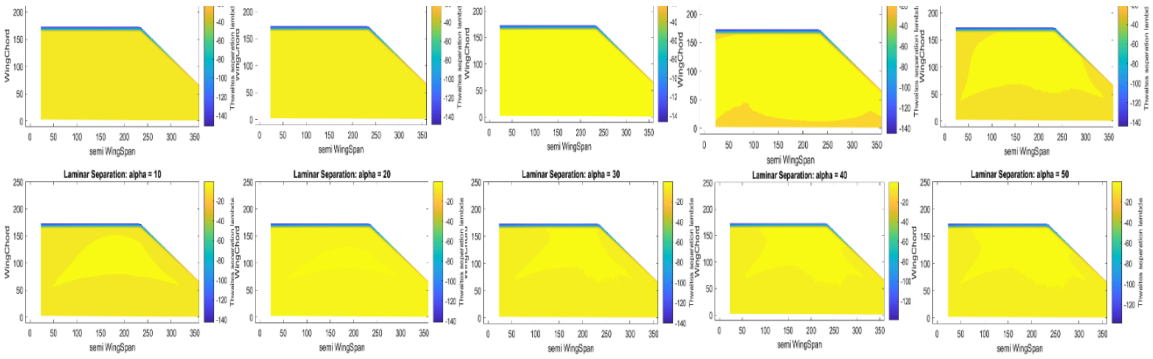

Figure 17: Laminar Separation criteria calculated using Thwaites equation.

This analysis was used while structuring the CL/CD values from VORLAX outputs to be used as inputs into the Python jump gliding model. The values were extrapolated from the VORLAX analysis range of angle of attack from [-30,50] to the python input range of [-

90, +90] angle of attack. This was done to ensure that the interpolation polynomial function built into the Python model will have sufficient data to reliably reproduce the VORLAX output against corresponding angle of attack. The extrapolation was done by converting the Lift-Drag data to the rotated Axial Force- Normal Force frame. The theoretical limits of Axial loading and Normal loading at -90 degrees and +90 degrees are established. These were used as hard limits and then the VORLAX data outputs were extrapolated to these limits for each angle of attack. All the modifications and operations done of the output were theoretically based and not done spuriously to obtain any convenient results. This does affect the efficacy of VORLAX data for the jump gliding model in Python, as the high angles of attack in jump phase. But the data is very well suited for modeling the glide phase, which is presented and discussed in Section 3.2.

3.2 Pynamics – Python Model

Jump gliding was modeled in Python using the Pynamics module developed by D. Aukes using Sympy, Numpy packages and the dynamics with Kane's method [30]. The model utilizes ballistic launch velocities, angle of launch and applied aerodynamic and spring forces to track the jump of robot with collapse of wings and subsequent gliding. The model is based on Kane's method of numerically deriving equations of motions, which is proven to be an accurate method with less computing requirements.

The model is based on calculating the magnitude and components of velocity of the several key points on the body from the applied initial conditions. These velocity

components are then used to formulate the primary variable of angle of attack and the aerodynamic forces acting on the wings as well as the spring torques being applied at the hinge joint. This formulation is presented as an expression made out of symbolic parameters. These symbolic expressions are then converted to a differential equation which is solved using an ordinary differential equation integrator found in the Python SciPy package. The solution found is then plugged into the symbolic expressions at each time step and plotted to obtain the robot response. Thus, the model has a constant exchange of information between symbolic and numeric structures.

Several challenges surfaced during integrating the VORLAX data into the Python model due to this interplay of different packages. Primary difficult in establishing a single jump-gliding model was found due to the difference in configuration of frames of reference in jumping phase and pure gliding phase. The ballistic jumping phase requires the angle of attack to be defined in such a way that the drag component of the wings is applied against the rotation of the wing around the hinge joint. While the angle of attack in the glide phase needs to be defined based on relative velocity due to the motion of body through the air and is simply applied at the wings in perpendicular and parallel direction components. The angle of attack formulation is important because it is the base parameter for the calculation of CL and CD, either for simple flat-plate aerodynamics equation or for the numeric VORLAX interpolation function. It was found in setup and testing of the initial models that this change of reference for definitions of angle of attack caused the results to be erroneous.

A strategy was adopted to separate the jump phase and gliding phase into two separate codes, with slight modifications in definition of frame of reference for velocity and angle of attack. The ballistic jump phase model utilizes the simple flat-plate model for modeling the collapse of tape spring hinges due to the air drag caused by the wings and is calculated from the user supplied initial conditions. The output of this simulation, primarily the state variables on the robot body at and near the maximum jump apex, is used as the initial condition for the second model. The second model focuses on the glide phase where the CL and CD values are calculated using the VORLAX numeric inputs. The simulation results are then extracted and compiled to obtain a complete picture.

The results obtained from the initial study of composite Python model using the flat-plate model for both jumping and gliding are presented below:

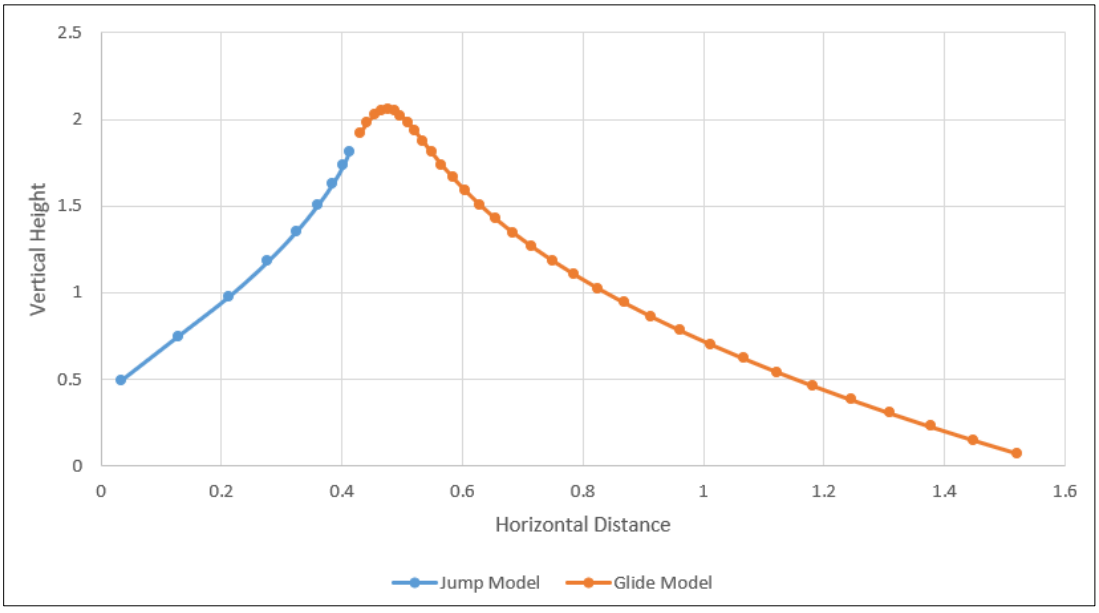

Figure 18: Initial composite Python model for jump gliding using flat-plate aerodynamic formulation.

The constant parameters such as mass of launcher parts, mass of wings, the initial conditions of the Python model are informed by the setup of experimental tests. This allows for the comparison of the two sets of results on a common basis. With the updated model using VORLAX input function for calculating CL/CD values, we obtain following jump gliding simulation (Figure 19).

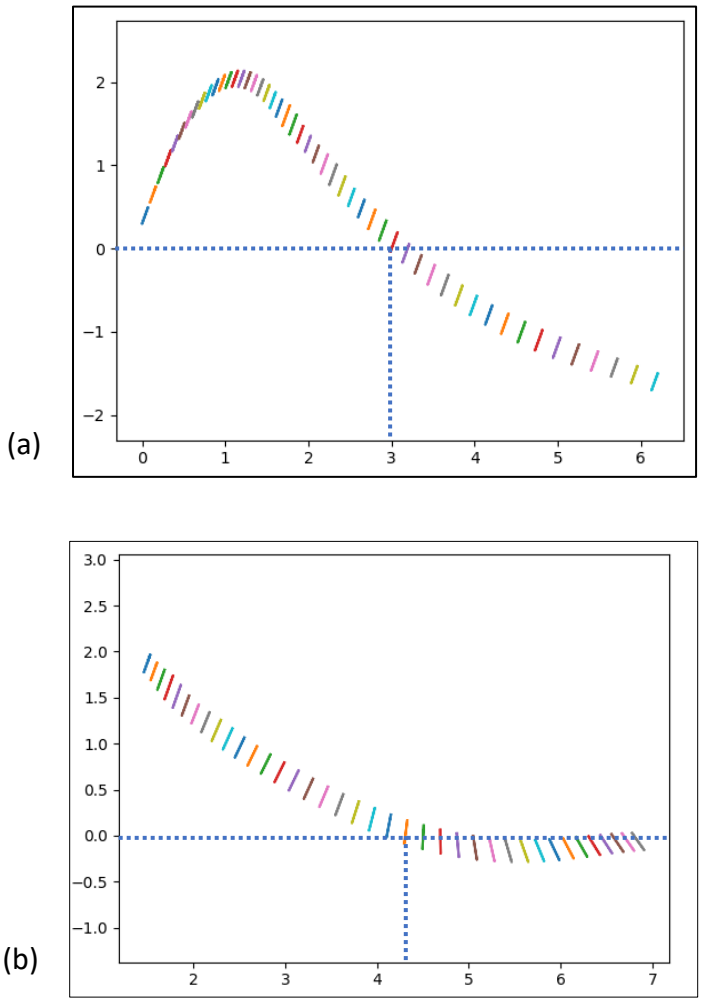

Figure 19: (a) Python model results with flat-plate model. (b) Glide model with VORLAX inputs using modified initial conditions.

We also observe that this new model highlights the difference between the theoretically formulated aerodynamic coefficients and the coefficients calculated from a cambered wing design using aerodynamic simulation tool.

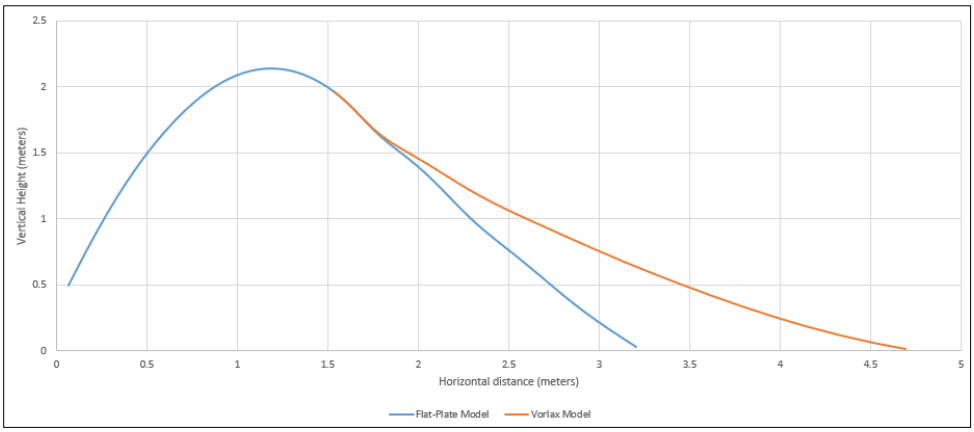

Figure 20: Python model simulation with VORLAX inputs.

Although the python model illustrates jump-gliding locomotion, its efficacy can only be gauged by the correlation of its outputs with the experimental results which is presented in Chapter 5. It is important to understand that the model assumes perfect world conditions with no external dynamic perturbations or imperfections in the prototype build. Moreover, the model assumes that the wings are point masses with no inertia, which cannot be replicated in real life. While the aerodynamic forces are modeled using the VORLAX coefficients with angle of attack parameter, the model currently does not include the pitching moments.

CHAPTER 4
TESTING & VALIDATION

4.1 Experimental Setup

The results of the Python model were tested and validated using a set of wing design geometry defined in the simulation process. The wings were made from inexpensive, easily available poster board. The purpose-made camber profile was laser-cut for maintaining design accuracy, with the poster board applied as a structural sheet tracing the profile with a balsa-wood spar for additional support (Figure 21). This enabled the wing to withstand the drag forces without buckling and completely transmit the load to the tape spring hinges during the jump phase. The wings weighed around 50 gm combined, which is only a fraction of total weight of the test article. But this weight can further be reduced by exploring other fabrication materials and methods. The tape spring hinges were obtained by truncating linkages of desired lengths from a carpenter's tape measure which is commonly found. The linkages were attached to the wings using small plastic rivets at equal lengths from the centerline. The linkages were attached to a 3D printed barrel using the same rivets, thus creating cantilever beam configuration out of the linkages on either side of the centerline.

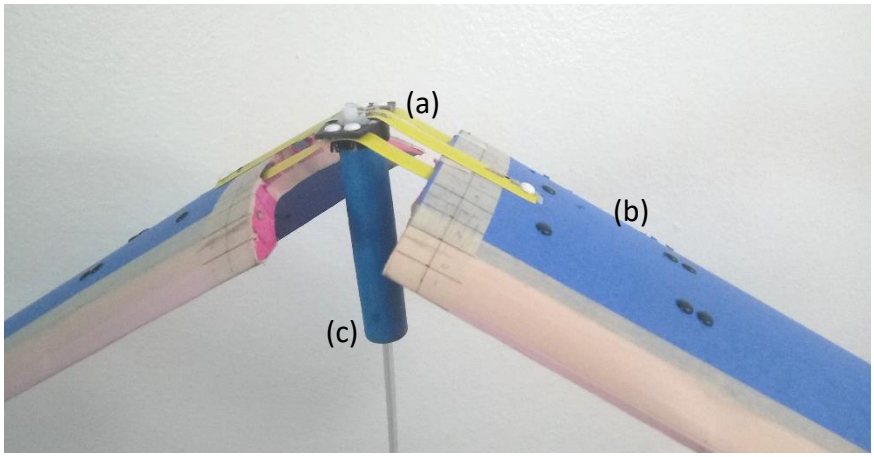

Figure 21: Prototype test article with (a) tape spring linkages; (b) cambered wings; (c) 3D printed barrel for launch mechanism.

The 3D printed barrel is a part of an external launcher mechanism which is utilized to mimic the ballistic launch condition of the robot jump. The launcher uses pressurized air to launch the barrel with release. The launcher is attached to a support structure which can be inclined to various angles with respect to the horizontal ground. To maintain a common threshold between all the different test configurations, the barrel is launched at 2 bar pressure and at a launch angle of 70 degrees. The study is aimed at the launch angle of only 70 degrees because it provides enough velocity horizontal component for transition and glide phase. This was found after testing the wing samples at various angles of 90, 80, 70 and 45 degrees. This launch angle also makes the adjustment of C.G of the wing easier to obtain reliable pitch stability.

The launch setup and subsequent analysis of experimental tests provided a velocity trace of the body throughout the locomotion. The launch velocity was found to be around 7 m/s with the glide velocities in the range of 2 m/s to 6 m/s, which is in complete agreement

with the seed values used for initial design analysis. These experimental results were used to update the simulation files and obtain the new analysis results for comparison.

The results from these tests were obtained by capturing the motion of body through the air and then processing the video using tracking marker glued to the body. The video analysis was done using Tracker, an open-source video analysis and computer modeling tool [31]. The setup of these tests was made sure to avoid any paralysis error by carefully placing the camera parallel to the plane of motion of the body, in front of a plain background. The lighting was made bright to achieve quality video frames. A calibration stick was placed in the background to enable correlation of pixel-to-length units in metrics.

The placement of C.G on the wing was an important parameter to achieve a stable jump-glide motion. The C.G was moved fore and aft using a small metal weight which was attached fore and aft of the linkage attachment points using a small attachment. This enabled the wings to be experimented with for different C.G locations which were changed by simply moving the dead weight on the extension along the centerline.

4.2 Experimental Results

The tests were conducted multiple times of the cambered wings as well as a flat-plate wing. The analysis results were extracted from the video Tracker and the marked (X, Y) coordinates along with velocity track were used to plot the results. These data points provided sufficient information for quantitative as well as qualitative comparison between the Python model.

The experimental test with the flat-plate wing failed to obtain any gliding after the jump phase. The reason behind this is suspected to be the failure of flat-plate geometry to generate sufficient CL values at such low velocity range. We can see from the Figure 22 that the wings are able to collapse during the jump phase but as soon as they begin the transition to glide phase, the wings toss over and falls. Any attempts to adjust the C.G created similar results.

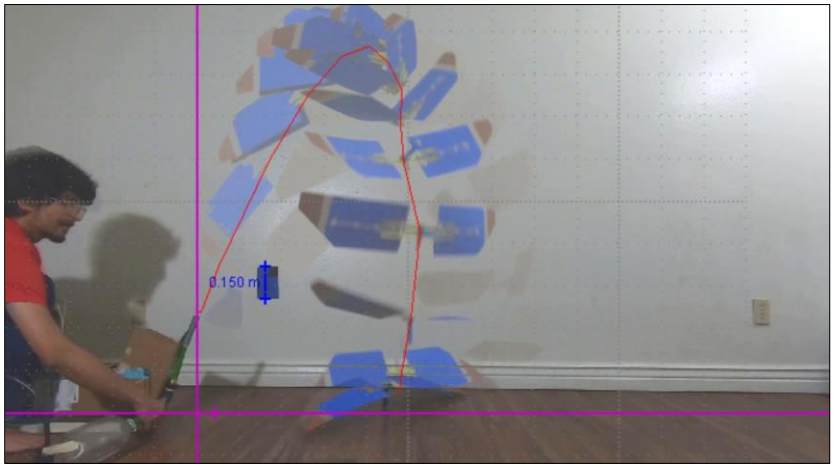

Figure 22: Experimental tests with zero camber, flat wings.

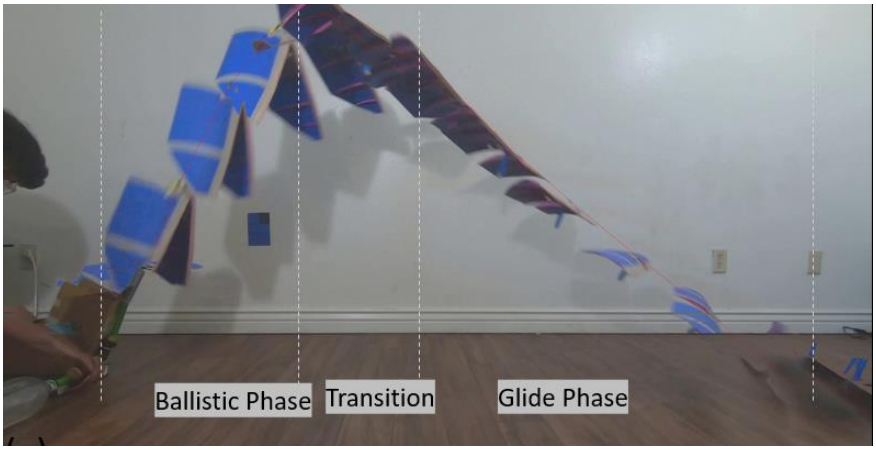

Figure 23: Experimental test with cambered wings showcasing successful jump gliding.

The tests with cambered wing profile were more successful and shown consistent jump gliding performance. Figure 24 shows the trajectory of wings with no changes in C.G. The maximum jump height achieved with collapse of wings was about 1.55 m with an average horizontal range of 2.7 m. In Figure 25, we can see that shifting the C.G aft slightly changed the trajectory of locomotion, while increasing the maximum jump height to 1.75 m. The range of jump glider is reduced to around 2.1 m with additional weight.

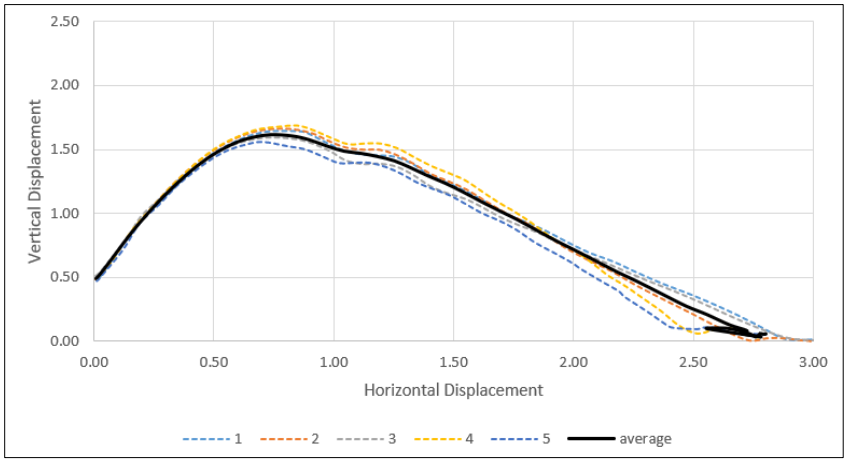

Figure 24: Jump gliding trajectory of a body with cambered wings.

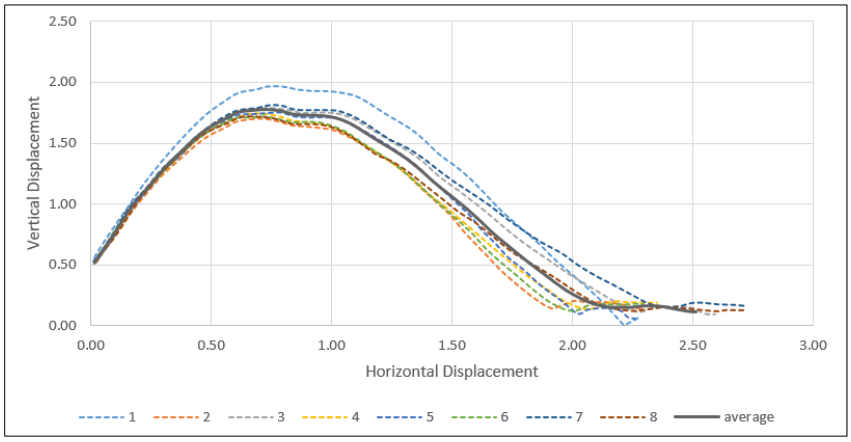

Figure 25: Jump gliding trajectory of a body with cambered wings with C.G shifted aft of the reference point.

We also observe an interesting response of tape spring hinge during the transition phase, as observed in model simulations. When the wings start deploying back, the opposite sense bending spring torque avoids the wing folding but induces minor flapping of the wings. These flapping oscillations die down quickly and the wings subsequently stabilize for the remainder of the glide.

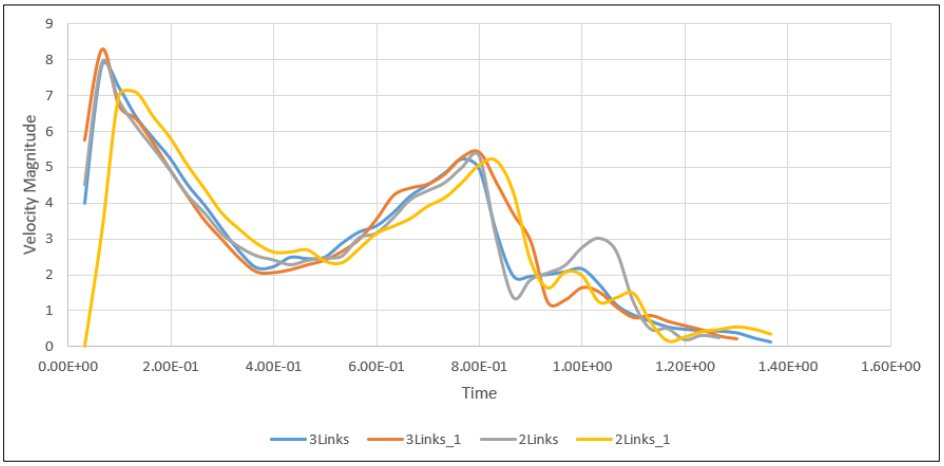

Figure 26: Velocity profile of a body with cambered wings through jump gliding

Along with the (X, Y) trajectory, we are also able to plot the velocity trace of the body through the jump gliding motion using video analysis. We can observe from Figure 26 that the velocity profile highlights various phases of the jump gliding motion very effectively. The initial peak of velocity is the launch velocity of the body with the subsequent drop in velocity representing the jump phase. As the body is ascending up, the kinetic energy is being converted to potential energy and it can be tracked by this loss of velocity. The small plateau in velocity curve shows the transition phase with the subsequent increasing velocity corresponds to the glide phase. We can see that the slope of this curve element is less which highlights the stable and controlled glide of the wings.

The velocity trace also becomes a good comparison parameter for understanding the Python model outputs and can be used to identify specific time steps of large deviations between the two.

When the Python model output is compared directly with the corresponding experimental test results, we obtain a quantitative comparison and evaluation of the Python model performance. In Figure 2, the flat-plate jump gliding model is compared to the experimental results of the flat wing. We can see that the composite model with jump and glide phase modeled separately showcases the best jump gliding trajectory, even with the failed experimental results.

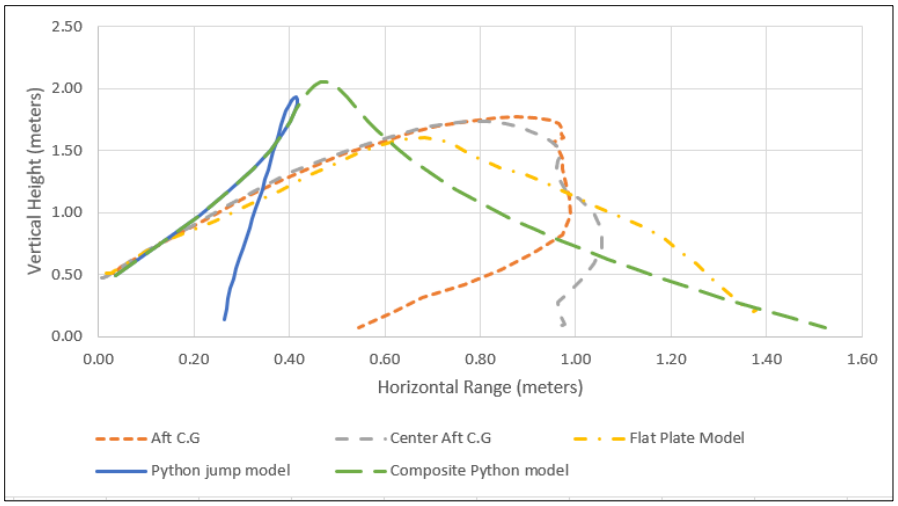

Figure 27: Comparison of Python simulation with experimental results for flat-plate wings.

The Figure 28 (a) compares the composite flat-plate model with the experimental results of cambered wing. We see that the two sets of results match well for a very small amount of time. But as the effect of cambered wing drag and the additional inertia shows up, they deviate from each other and there is no correlation between the two. Also, we observe that the flat-plate model underestimates the jump gliding performance by quite some margin.

This result presents a compelling argument for inclusion of geometry-specific aerodynamic simulation data in the jump gliding dynamics model. We can see similar trends in the comparative analysis of the velocity trace of the Python model and the experimental results.

Figure 28(b) compares the results of experimental cambered wing with that of composite Python model utilizing VORLAX inputs. It is observed that the Python model, updated with modified initial conditions and constant variables, overestimates the jump gliding performance. Glide Ratio is a parameter which is defined as a ratio between the horizontal distance covered to the corresponding drop in altitude for the flying body. The comparison of glide ratios between the experimental results and Python simulation results in glide phase is presented in Table 3. We can see that the Python model with flat-plate formulation has a lower glide ratio than the experimental result of cambered wing, while the VORLAX Python model has a higher glide ratio. We can observe from the trajectory plots that the simulation model and experimental tests agree well in the initial jump phase. But as the experimental trajectory achieves its peak height, the model trajectory keeps gaining height. This advantage in height is then converted to a greater gliding range for the Python model.

Legend	Horizontal Range	Vertical height loss	Glide Ratio
Cambered Wing	1.73	1.48	1.168919
Aft C.G Cambered Wing	1.47	1.7	0.864706
Flat-plate model	1.671	1.97	0.848223
VORLAX model	3.16	1.97	1.604061

Table 3: Glide ratios calculated from simulation and experimental results.

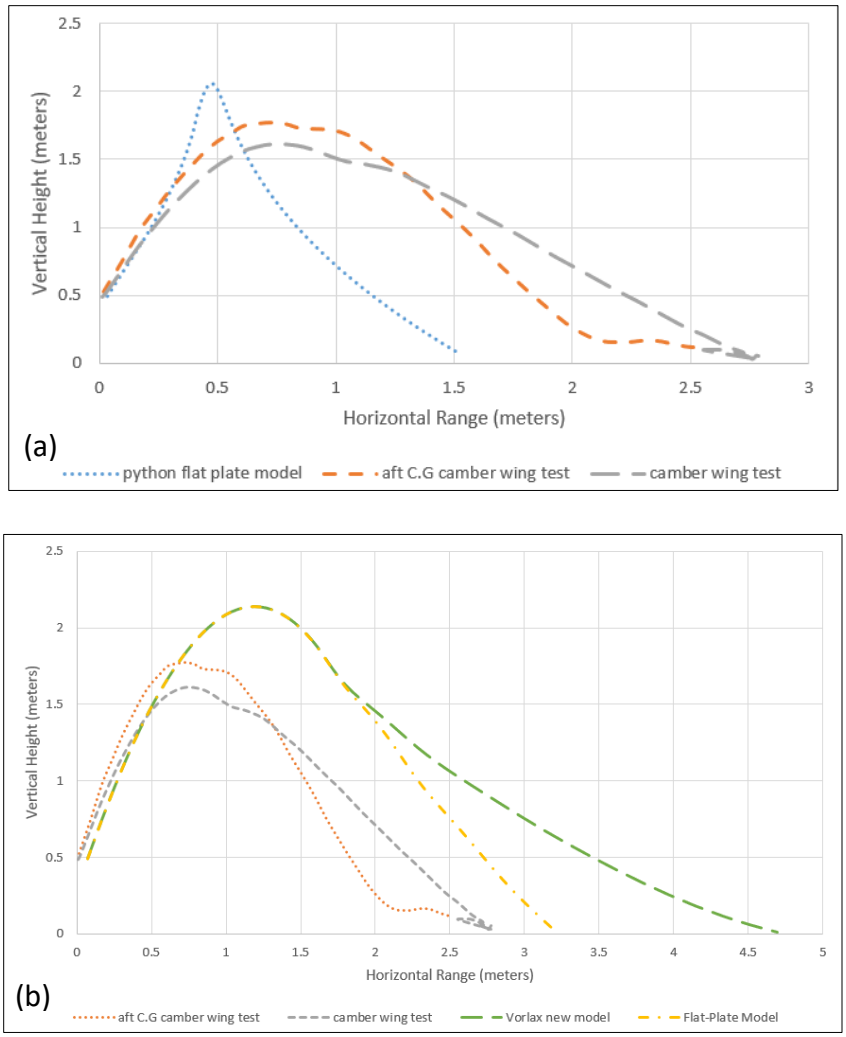

Figure 28: (a) Comparison of flat-plate Python simulations with the experimental results from the cambered wings. (b) Comparison of results between Python simulations with VORLAX inputs and experimental results from cambered wings.

CHAPTER 5
CONCLUSION

5.1 Discussion of Results

It is evident from the presented work and the results obtained from the analysis that there is a requirement for integrating special aerodynamic tools for modeling of such hybrid locomotion strategies. The results also clearly prove that such complex locomotion gaits operate far outside the assumption regime of the aerodynamic flat-plate theory and the corresponding formulations. These differences are made more evident due to the larger scale of the robot and the special wing design solutions to accommodate it.

The application of a passive self-deploying mechanism for collapse of wings using the tape-springs is successfully presented. While the focus of this project was the aerodynamic design accompanying this tape-spring hinge mechanism, the results prove that the collapse of wings can be achieved without contributing to any weight or components to the platform. The design of an aerodynamic system around such a mechanism is one of the major contributions of this project.

The presented aerodynamic design of the wings also provide a useful insight in the design of low aspect ratio, high camber wings and the post-processing required for using the resulting analysis. It is shown from the presented work that a successful aerodynamic package can be built for multi-domain, multi-modal locomotion strategies with heavy constraints and limited tools.

While the project hasn't been able to provide a single, unified model for simulating the jump gliding, it is evident from the compiled model results that the modifications and strategies used are steps in the right direction. The simple model presented here may be used as a platform for building the dynamic complexity over time.

The presented Python model also provides a unique highlight of compiling symbolic, numeric and mathematical package structures. This provides of an opportunity to developing new design workflows for simulation and analysis with input parameters from different domains. This would enable analysis of multiple iterations for a given system at initial stages of design process, which can then be used to shortlist only the best performing designs. It helps is reducing the design errors and saves time in the process.

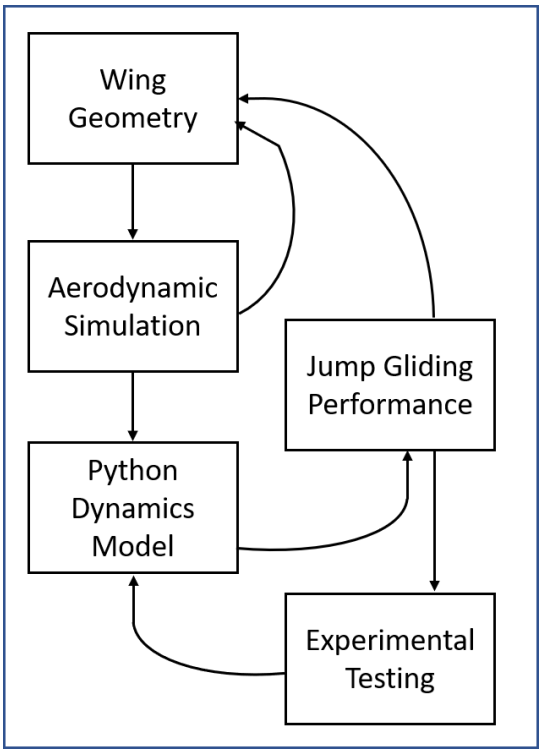

Figure 29: Design Workflow presented for jump gliding robots.

5.2 Future Work

There have been a few areas identified from the presented document for future work. Some immediate improvements can be made in the Python model in the process of interpolation and processing of the numeric aerodynamic data from VORLAX. The whole design process can be codified into a single platform that will accommodate the definition of wing geometry, generation of input file and running the VORLAX results with parsing these results for the numeric data required for the jump gliding dynamics model. This will help save time against manually switching between different platforms and also help with better management of input files and generated log files.

The python model can also be modified to include pitching moments acting at the reference point and using them to analyze the in-flight dynamic response of the body to various sets of initial conditions and wing designs. This will help in simulating the body attitude through transition and glide phase along with providing quantitative data on the dynamic response of changes in C.G.

A few aerodynamic improvements can be made in the wing design with application of twist at the wing tip for extracting better efficiency and dynamic performance. Any reduction in the weight of the biped platform will directly help in easing the lift requirements on the wings. This will mean the applied maximum camber can be reduced and the aerodynamic performance can be modelled better with simpler interpolant functions as non-linearities are avoided. This will also help in easier integration of aerodynamic data and provide better efficacy form the dynamics model.

BIBLIOGRAPHY

[1] U. M. Norberg, “Evolution of Vertebrate Flight : An Aerodynamic Model for the Transition from Gliding to Active Flight Author (s): Ulla M . Norberg Source : The American Naturalist , Vol . 126 , No . 3 (Sep ., 1985), pp . 303-327 Published by : University of Chicago,” *Am. Nat.*, vol. 126, no. 3, pp. 303–327, 2016.

[2] R. Dudley, G. Byrnes, S. P. Yanoviak, B. Borrell, R. M. Brown, and J. A. McGuire, “ Gliding and the Functional Origins of Flight: Biomechanical Novelty or Necessity ? ,” *Annu. Rev. Ecol. Evol. Syst.*, vol. 38, no. 1, pp. 179–201, 2007.

[3] M. Kovač, J. C. Zufferey, and D. Floreano, “Towards a self-deploying and gliding robot,” *Fly. Insects Robot.*, pp. 271–284, 2010.

[4] M. Sharifzadeh and D. M. Aukes, “Curvature-Induced Buckling for Flapping-Wing Vehicles,” *(Submitted)*, no. i, 2019.

[5] T. Shafa, “Design, Model, and Control of a Low-Cost 3 Degree of Freedom Balancing Laminate Leg with an Actively Controlled Ankle Using Fundamental Controls Concepts,” Arizona State University, 2020.

[6] M. Kovač, Wassim-Hraiz, O. Fauria, J. C. Zufferey, and D. Floreano, “The EPFL jumpglider: A hybrid jumping and gliding robot with rigid or folding wings,” *2011 IEEE Int. Conf. Robot. Biomimetics, ROBIO 2011*, pp. 1503–1508, 2011.

[7] A. Vidyasagar, J. C. Zufferey, D. Floreano, and M. Kovač, “Performance analysis of jump-gliding locomotion for miniature robotics,” *Bioinspiration and Biomimetics*, vol. 10, no. 2, pp. 1–12, 2015.

[8] A. Beck, V. Zaitsev, U. Ben Hanan, G. Kosa, A. Ayali, and A. Weiss, “Jump stabilization and landing control by wing-spreading of a locust-inspired jumper,” *Bioinspiration and Biomimetics*, vol. 12, no. 6, 2017.

[9] V. Zaitsev, O. Gvirsman, U. Ben Hanan, A. Weiss, A. Ayali, and G. Kosa, "Locust-inspired miniature jumping robot," *IEEE Int. Conf. Intell. Robot. Syst.*, vol. 2015-Decem, pp. 553–558, 2015.

[10] R. Armour, K. Paskins, A. Bowyer, J. Vincent, and W. Megill, "Jumping robots: A biomimetic solution to locomotion across rough terrain," *Bioinspiration and Biomimetics*, vol. 2, no. 3, 2007.

[11] L. Daler, S. Mintchev, C. Stefanini, and D. Floreano, "A bioinspired multi-modal flying and walking robot," *Bioinspiration and Biomimetics*, vol. 10, no. 1, 2015.

[12] A. L. Desbiens, M. T. Pope, D. L. Christensen, E. W. Hawkes, and M. R. Cutkosky, "Design principles for efficient, repeated jumpgliding," *Bioinspiration and Biomimetics*, vol. 9, no. 2, 2014.

[13] M. A. Woodward and M. Sitti, "MultiMo-Bat: A biologically inspired integrated jumping-gliding robot," *Int. J. Rob. Res.*, vol. 33, no. 12, pp. 1511–1529, 2014.

[14] D. Wei, T. Gao, Z. Li, X. Mo, S. Zheng, and C. Zhou, "Hybrid inspired research on the flying-jumping locomotion of locusts using robot counterpart," *Front. Neurorobot.*, vol. 13, no. October, pp. 1–13, 2019.

[15] N. T. Truong, H. V. Phan, and H. C. Park, "Design and demonstration of a bio-inspired flapping-wing-assisted jumping robot," *Bioinspiration and Biomimetics*, vol. 14, no. 3, 2019.

[16] J. W. Knaup and D. M. Aukes, "IDETC2019-98109," 2019.

[17] M. Ziv-El *et al.*, "Development and characterization of DehaloR 2, a novel anaerobic microbial consortium performing rapid dechlorination of TCE to ethene," *Appl. Microbiol. Biotechnol.*, vol. 92, no. 5, pp. 1063–1071, 2011.

[18] G. Lighthouse and D. Aukes, "Extending the Jumping Range of a Small Robot via Collapsible Gliding Wings," no. April, pp. 1–8, 2019.

[19] J. N. Footdale and T. W. Murphey, “Mechanism Design and Testing of a Self-Deploying Structure Using Flexible Composite Tape Springs,” *Proc. 42nd Aerosp. Mech. Symp.*, pp. 1–13, 2015.

[20] K. A. Seffen and S. Pellegrino, “Deployment dynamics of tape springs,” *R. Soc.*, 1999.

[21] P. Dees, “Hang glider design and performance,” *10th AIAA Aviat. Technol. Integr. Oper. Conf. 2010, ATIO 2010*, vol. 3, no. September, pp. 1–13, 2010.

[22] A. SMITH, “High-lift aerodynamics /37th Wright Brothers Lecture/,” vol. 12, no. 6, 1974.

[23] J. L. Lin, C. Y. Wei, and C. Y. Lin, “Aerodynamic performance of thin wings at low Reynolds numbers,” *Aircr. Eng. Aerosp. Technol.*, vol. 81, no. 1, pp. 51–58, 2009.

[24] M. V. Cook and M. Spottiswoode, “Modelling the flight dynamics of the hang glider,” *Aeronaut. J.*, vol. 110, no. 1103, pp. 1–20, 2006.

[25] B. Etkin and T. Teichmann, “ Dynamics of Flight: Stability and Control ,” *Phys. Today*, vol. 12, no. 9, pp. 54–56, 1959.

[26] L. R. Miranda, R. D. Elliott, and W. M. Baker, “Supersonic Flow Applications,” 1977.

[27] MILGRAM JH, “Section data for thin, highly cambered airfoils in incompressible flow,” *NASA Contract. Reports*, no. July 1971, 1971.

[28] “Airfoil Tools.” http://airfoiltools.com/search/index.

[29] B. Thwaites, *Incompressible Aerodynamics*. Clarendon Press, Oxford, 1960.

[30] D. Aukes, “Pynamics.”. https://github.com/idealabasu/code_pynamics .

[31] D. Brown, “Tracker.” [Online]. Available: https://physlets.org/tracker/.